

2024 International Conference on Science and Technology, Modern Education and Management (TMEM 2024)

Research on Self-supporting Structure in Bird Nests

Yuming Chen^{1a}, Yifang Xu^{1b} & Yiran Yao^{1c}

¹ Basis International School Nanjing, Nanjing, Jiangsu, China

^a 3258240133@qq.com

^b ttamymc@yeah.net

^c yrharryyao@icloud.com

Abstract

The mystery behind the bird nest's construction is not well understood. Our study focuses on the stability of a self-supporting nest-like structure. Firstly, we derived a stable/unstable phase boundary for the structure at the fixed coefficient of friction with varying geometrical parameters through force analysis. Structures with a lower height and greater friction coefficient between rods are more stable. The theoretical phase boundary matched the experiment results well. Then we investigate the nest structure's stability under applied weight. Static structures with lower height and more rods (five>four>three) are more stable. Our theory also predicts a transition from plastic phase to elastic phase. These theoretical predictions are all confirmed by experiment. In the experiment, we also find that wet rod structures are more stable than dry ones. The structures can support up to 100 times of its weight.

Keywords

Self-supporting, Bird Nest, Stability, Plastic Phase, Elastic Phase, Phase Transition

1. Introduction

Birds choose simple elements from their environment and synthesize them into their nests (Figure 1). However, the mystery behind the bird nest's construction is still not well understood (Weiner, Bhosale, Gazzola & King, 2020). Siobhan Roberts (Siobhan, 2020) simplifies a nest to random packing of sticks (slender grains) and hypothesizes that "the nest state" results from the "jamming" of its elements (Andrea & Sidney, 2010) that prevent them from falling apart. Inspired by these works, we will study the mechanics of a nest structure made of bamboo sticks and try to answer how and why birds can build a stable structure by merely packing.



Figure 1. Bird Nest (from Internet)



Figure 2. Nest is not a Stick Bomb

We will not regard a nest as a stick bomb (Popular Science Matters, 2020) (explodes and releases the elastic potential energy when falls to the ground), as shown in Figure 2, with stored elastic potential energy to keep itself stable. In a stick bomb, it is the external force that causes the elastic deformation which produces the normal forces and produces the friction to hold the whole structure. In this aspect, we suppose that the normal forces inside a nest arise to resist its own gravity and balance the structure. Neither will we use a container to hold the random sticks together (Yashraj, Nicholas, Butler, Seung, Mattia & Hunte, 2022). Like a real bird does, we try to obtain a stable structure that can stand by itself by merely packing. Then, we find such a self-supporting structure with only a few sticks (see figure 3 and 4), where the normal force inside a nest arises to resist its own gravity. To build a practical bird nest, our structure may act as the base of the nest that supports the weight of a bunch of filling sticks and the birds and eggs.

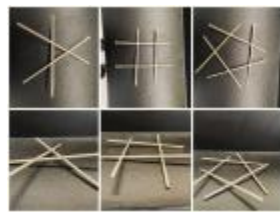


Figure 3. Build the Structure



Figure 4. Rod Structures

Our study focuses on the stability of this self-supporting nest structure. We derive the stability conditions and obtain a phase diagram of a free nest structure by force analysis and verify the phase diagram by experiment. Then we test the nest structure's stability under applied weight. Ultimately, this paper aims to explore new possibilities of the potential application of the nest structure in architecture, packaging, and other fields of industry. By analyzing its properties, we aim to pave the way for more sustainable and resilient materials.

2. Static Stability of Free Bird Nest Structure

Some structures are able to stand steadily whereas others collapse or slide down to a stable level. To derive the physical conditions that allow rods to stand stable, we analyze the forces and torques in this system. First, we theoretically analyze the forces in the system and mathematically derive the conditions. Then we will verify the conditions through experiments.

2.1 Theory

2.1.1 Variables

Table 1. Variable List Symbol Description

L	Length of the Rod
d_1, d_2, d_3	Length of lower, middle, and upper segment
m	Mass of the rod
t	Thickness (diameter) of rod
n	Number of rods
θ	Angle between rods and the ground
α	Interior Angle of a regular n-gon
μ	Friction between rods
μ'	Friction between rods and table
h	Height of rods

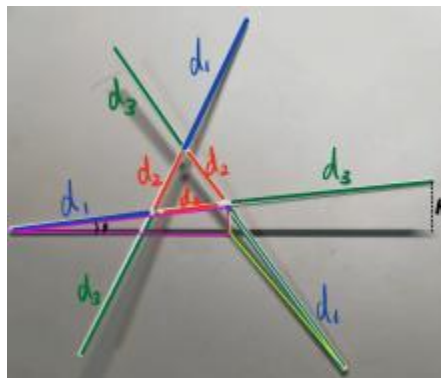


Figure 5. Visual Representation of Variables

2.1.2 Angle with Ground

All variables mentioned in the following text are represented in table 1. In figure 5, the angle θ each rod makes with the ground can be determined geometrically. The height of the pink triangle on the left is $(d_1 + d_2) \sin \theta$, and the height of the green triangle on the right is $d_1 \sin \theta$. The two heights differ by the diameter of the rod, t .

$$d_1 \sin \theta + d_2 \sin \theta = d_1 \sin \theta + t \quad (1)$$

$$\sin \theta = \frac{t}{d_2} \quad (2)$$

Thus, the height of a structure is

$$h = L \sin \theta = L \frac{t}{d_2} \quad (3)$$

2.1.3 Force and Torque Analysis

There are 7 forces in total on the rod: 3 pairs of normal forces and friction forces, along with gravity. If the structure is in equilibrium, forces and torques are balanced for each rod. To simplify, we only investigate rod structures that are symmetrical. (Yao, Liu, Yang, Xiao & Zheng, 2024)

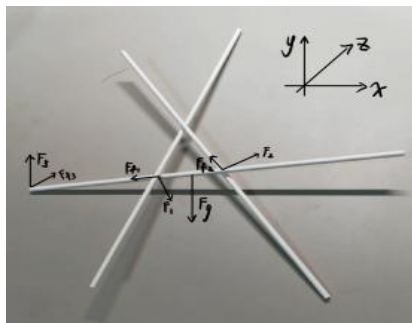


Figure 6. Free Body Diagram

The weights of the rods are distributed evenly across the three contact points with the ground. Thus, $F_3 = mg$ and $F_{f3} \leq \mu' mg$. As the structure is symmetric, $F_1 = F_2$ and $F_{f1} = F_{f2}$.

We establish a 3-D coordinate system. The x-z plane is the table. +x is from left to right, and +z is from closer to further. y is the height from the ground. We then represent the forces as vectors.

$$\begin{aligned}
\vec{F}_3 &= [0 \quad mg \quad 0], \\
\vec{F}_{f3} &= [F_{f3x} \quad 0 \quad F_{f3z}], \\
\vec{F}_g &= [0 \quad -mg \quad 0], \\
\vec{F}_1 &= [-F_1 \sin\theta \cos\alpha \quad -F_1 \cos\theta \quad -F_1 \sin\theta \sin\alpha], \\
\vec{F}_{f1} &= [-F_{f1} \cos\theta \quad -F_{f1} \sin\theta \quad 0], \\
\vec{F}_2 &= [F_2 \sin\theta \cos\alpha \quad F_2 \cos\theta \quad -F_2 \sin\theta \sin\alpha], \\
\vec{F}_{f2} &= [F_{f2} \cos\theta \cos\alpha \quad F_{f2} \sin\theta \quad -F_{f2} \cos\theta \sin\alpha].
\end{aligned} \tag{4}$$

Take the contact point to the ground as the center of rotation. The radius of each force can be represented as the following vectors:

$$\begin{aligned}
\vec{R}_F &= \vec{R}_{Ff3}, \\
\vec{R}_{F1} &= \vec{R}_{Ff1} = [d_1 \cos\theta \quad d_1 \sin\theta \quad 0], \\
\vec{R}_{Ff2} &= \vec{R}_{Ff2} = [(d_1 + d_2) \cos\theta \quad (d_1 + d_2) \sin\theta \quad 0], \\
\vec{R}_G &= [L/2 \cos\theta \quad L/2 \sin\theta \quad 0].
\end{aligned} \tag{5}$$

Forces and torques need to be balanced out for the structure to stay in equilibrium. By $\sum \vec{F} = \vec{0}$ and $\sum \vec{R} \times \vec{F} = \vec{0}$, we can set up the following system of equation.

$$\begin{cases}
-F_1 \sin(\theta) \cos(\alpha) + F_2 \sin(\theta) \cos(\alpha) - F_{f1} \cos(\theta) - F_{f2} \cos(\alpha) \cos(\theta) + F_{f3x} = 0, & (6) \\
F_{f1} \sin(\theta) + F_{f2} \sin(\theta) = 0, & (7) \\
-F_1 \sin(\alpha) \sin(\theta) - F_2 \sin(\alpha) \sin(\theta) + F_{f2} \sin(\alpha) \cos(\theta) + F_{f3z} = 0, & (8) \\
F_1 d_1 \sin(\alpha) \sin^2(\theta) + F_2 (d_1 + d_2) \sin(\alpha) \sin^2(\theta) - F_{f2} (d_1 + d_2) \sin(\alpha) \sin(\theta) \cos(\theta) = 0, & (9) \\
-F_1 d_1 \sin^2(\theta) \cos(\alpha) + F_1 d_1 \cos^2(\theta) + F_2 (d_1 + d_2) \sin^2(\theta) \cos(\alpha) - F_2 (d_1 + d_2) \cos^2(\theta), & \\
-F_{f2} (d_1 + d_2) \sin(\theta) \cos(\alpha) \cos(\theta) - F_{f2} (d_1 + d_2) \sin(\theta) \cos(\theta) + L g m \cos(\theta) / 2 = 0. & (11)
\end{cases}$$

The first three equations are derived from force equilibrium in the x, y, and z direction respectively. The latter three equations are derived from torque equilibrium in the x, y, and z directions respectively. With $F_1 = F_2 = F_N$ and $F_{f1} = F_{f2} = F_f$, we can then simplify the set of equations to the following:

$$\begin{cases}
(F_{f3x} - F_f \cos\theta(1 + \cos\alpha) = 0, & (12) \\
F_{f3z} - 2F_N \sin\theta \sin\alpha + F_f \cos\theta \sin\alpha = 0, & (13) \\
F_N d_1 (\cos^2\theta - \sin^2\theta \cos\alpha) + F_N (d_1 + d_2) (\sin^2\theta \cos\alpha - \cos^2\theta) & \\
- F_f (d_1 + d_2) \sin\theta \cos\theta (1 + \cos\alpha) + \frac{L m g \cos\theta}{2} = 0. & (16)
\end{cases}$$

We can derive the condition for μ by adding equation (14) and equation (15).

$$F_f = F_N \frac{2d_1+d_2}{d_1+d_2} \tan\theta. \quad (17)$$

By $F_f \leq \mu F_N$,

$$\mu \geq \frac{2d_1+d_2}{d_1+d_2} \frac{t}{\sqrt{d_2^2-t^2}}. \quad (18)$$

Substitute equation (17) into equation (16),

$$F_N = \frac{Lmg\cos\theta}{4d_1\sin^2\theta(1+\cos\alpha)+2d_2}. \quad (19)$$

Substitute equation (19) into equation (17),

$$F_f = \frac{Lmg\sin\theta(2d_1+d_2)}{(4d_1\sin^2\theta(1+\cos\alpha)+2d_2)(d_1+d_2)}. \quad (20)$$

Substitute equation (17) into equation (12) and equation (13),

$$F_{f3x} = F_N \frac{(2d_1+d_2)\sin\theta(1+\cos\alpha)}{d_1+d_2}, \quad (21)$$

$$F_{f3z} = F_N \frac{d_2\sin\theta\sin\alpha}{d_1+d_2} \quad (22)$$

Combining the components of F_{f3} , we can derive the condition,

$$\mu'^2 \geq \frac{L^2(d_2^2\sin^2\alpha+(2d_1+d_2)^2(1+\cos\alpha)^2)\sin^2\theta\cos^2\theta}{4(d_1+d_2)^2(2d_1(1+\cos\alpha)\sin^2\theta+d_2)^2}. \quad (23)$$

Equation (18) is the condition for static friction coefficient between rods μ , and equation (23) is the condition for static friction coefficient between rods and the table

μ' . When μ' is big enough, the condition for μ would be the limiting factor, and the stability of the structure will depend on d_1 and d_2 only.

2.1.4 Energy Analysis

Figure 7 We attempt to analyze the rods structure's behavior through potential energy level.

Consider the following structure. The rod on the left is supported by the rod on the right. Their point of contact with the ground is fixed, so what distance of x gives the maximum energy?

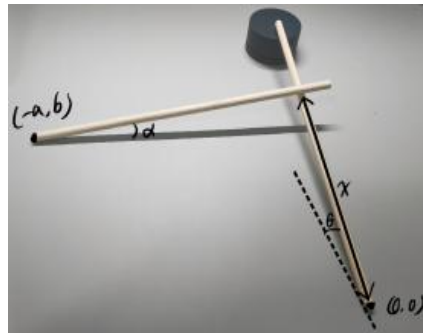


Figure 7. Two Rods Structure and Variables

$$\tan \alpha = \frac{x \sin \theta}{\sqrt{a^2 + (x \cos \theta - b)^2}} \quad (24)$$

The potential energy of the rod A

$$E \propto y_{o_a} = \frac{L}{2} \sin \alpha = \frac{L}{2} \frac{x \sin \theta}{\sqrt{a^2 + b^2 + x^2 - 2bx \cos \theta}} \quad (25)$$

We solve for extremes by taking the derivative

$$\frac{dy_{o_a}}{dx} = \frac{Lgm(a^2 + b^2 - bxcos\theta)sin\theta}{2(a^2 + b^2 - 2bxcos\theta + x^2)^{\frac{3}{2}}} \quad (26)$$

One local extrema exists at

$$x = \frac{a^2 + b^2}{bcos\theta} \quad (27)$$

Figure 8 shows the potential energy of rod A as a function of x , the distance from the intersection to the landing point of rod B. There is one global maxima. The system's potential energy will drop rapidly as x decreases, and will drop quickly as x increases.

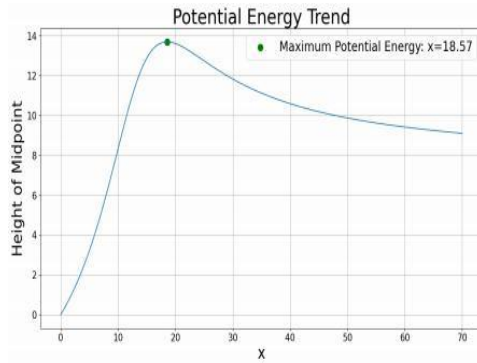


Figure 8. Potential Energy Trend of Rod A, $L = 30$, $a = 5$, $b = 15$, $\theta = \frac{\pi}{6}$

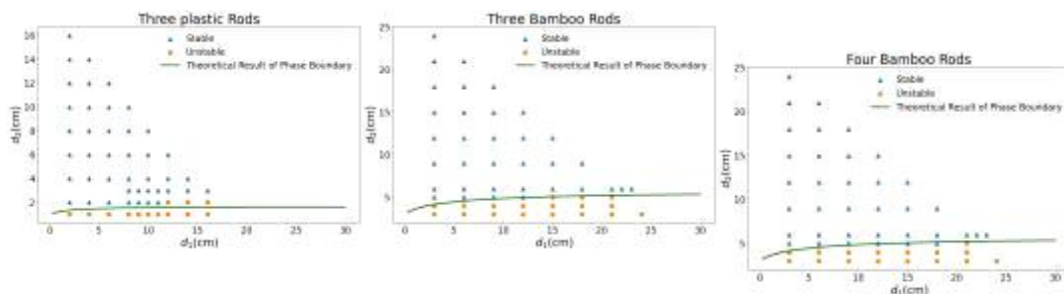
2.2 Experiments

2.2.1 Experiment Results

We test our theoretical prediction with structures of different materials, lengths, diameters, and number of rods. We vary the combination of d_1 and d_2 and check whether the structure can self-support. We then compare the experiment results to theoretical prediction. Under sufficient μ' , we focus only on the condition for μ . Structures with d_1 and d_2 above the curve are stable whereas those below is unstable. Parameters of test cases are shown below in Table 2.

Table 2. Summary of Test Cases

Test Case	Number of Rods	Material	Diameter (cm)	L (cm)	μ
Case 1	3	Plastic	0.30	20	0.36
Case 2	3	Bamboo	0.80	30	0.27
Case 3	4	Bamboo	0.80	30	0.27



(a) Case 1: Three Plastic Rods (b) Case 2: Three Bamboo Rods (c) Case 3: Four Bamboo Rods

Figure 9. Stability Diagram for Theoretical and Experimental Results

Figure 9 The theoretical stability boundary is mainly determined by μ and d_2 , see equation (18),

and is independent of mass and number of rods—the experiment result of three and four rods is almost the same. Unstable experimental data may fall beyond the curve. The reason is that the stable structures near the boundary is rather weak and can easily be disturbed by very small disturbance. In conclusion, the theoretical and experimental results matched. Theory better predicted the stability of bamboo rods than plastic rods. This is likely because the thin plastic rods deformed in shape, which affected the friction coefficient.

3. Static Stability of Bird Nest Structure under Applied Weight

3.1 Theory

A stable structure should maintain its shape when holding weights. The objective of this section is to investigate the relationship between applied weight and structural deformation. We aim to quantify this ability by applying incremental loads on the top of rod structures and subsequently measuring the corresponding decrease in height.

We introduce the new force from applied weight besides the force vectors in equation (4). F_3 changes alongside, restoring balance of forces.

$$F_a = \left[0 - \frac{Mg}{n} 0 \right] \quad (28)$$

$$F'_s = [0 \quad mg + Mg \quad 0].$$

We need to resolve the balance of torque. The radius of applied force is

$$R_a = [L \cos \theta \quad L \sin \theta \quad 0] \quad (29)$$

The new force doesn't affect condition for μ (Equation (18)), but would alter condition for μ' .

$$F'_N = \frac{L(M/n+m/2)g \cos \theta}{2d_1 \sin^2 \theta (1 + \cos \alpha) + d_2}. \quad (30)$$

$$\mu'^2 \geq \frac{L^2 \left(\frac{M/n+m/2}{M/n+m} \right)^2 (d_2^2 \sin^2 \alpha + (2d_1 + d_2)^2 (1 + \cos \alpha)^2) \sin^2 \theta \cos^2 \theta}{(d_1 + d_2)^2 (2d_1 (1 + \cos \alpha) \sin^2 \theta + d_2)^2} \quad (31)$$

3.2 Experiment Procedure

We apply force along the rod and measure the minimum angle that the rod can make with the ground. As shown in the figures, we can calculate and take account of the frictional forces the rods make with the ground Figure 10 and Figure 11.



Figure 10. Friction Coefficient Measurement

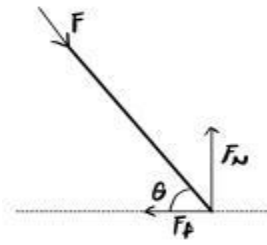


Figure 11. Friction Measurement

Thus, we can derive μ' from the angle with ground:

$$\mu' = \frac{F_f}{F_N} = \frac{F \cos \theta}{F \sin \theta} = \cot \theta. \tag{32}$$

Figure 12 Other than measuring the friction of the structures, we also use the Bending Method (Song, Sun, Liu, & Li, 2016) to calculate the Young's Modules of dry and wet rods. We first place the rod on two thin blades and hang a weight load at the middle of the rod. Young's modules can be calculated as

$$Y = \frac{\Delta m g l^3}{12 \pi r^4 \Delta z} \tag{33}$$

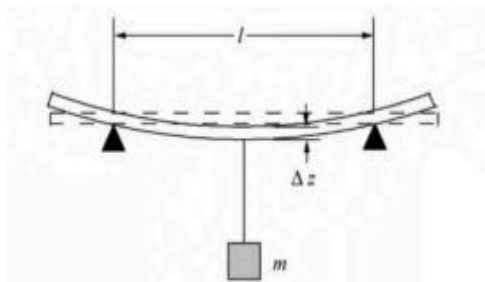


Figure 12. Young's Modules Measurement

The parameters of the rods we use are shown in the Table 3.

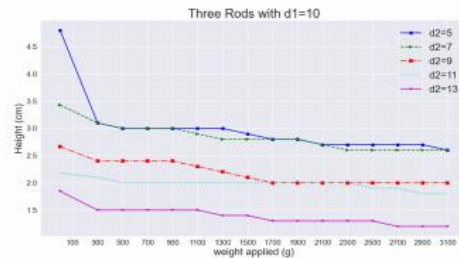
Table 3. Values of Various Rod Types

Type of Rod	r (cm)	Δm (kg)	m (g)	l (cm)	Δz (cm)	Y (Pa)
Wet Rods	0.80	2.6	9.0	30.0	1.2	5.7×10^9
Dry Rods	0.80	2.6	9.75	30.0	1.0	7.2×10^9

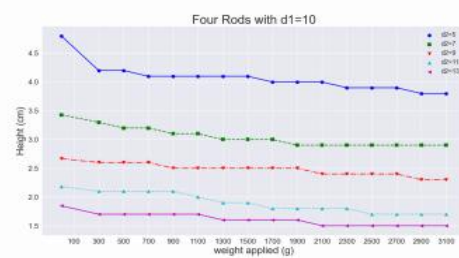
For three-rods, four-rods, and five-rods structures, we set $d_1 = 10\text{cm}$ and vary d_2 from 5 cm (structures with $d_2 < 5$ cannot stand on its own) to 13 cm, increasing 2 centimeters at a time. We also soak rods into water overnight to observe the effect of moisture.

3.3 Experiment Results and Analysis

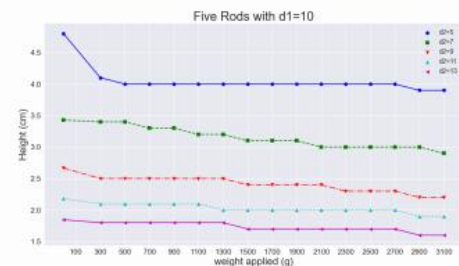
The three figures below are experiment results for $n=3, 4$ and 5.



(a) Three Dry Rods, experiment date June 4th



(b) Four Dry Rods, experiment date June 4th

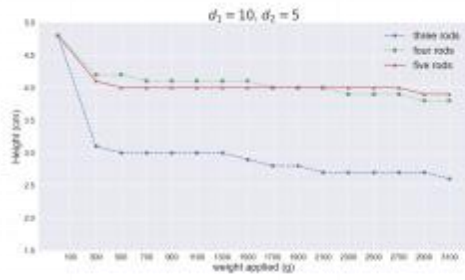


(c) Five Dry Rods, experiment date June 4th

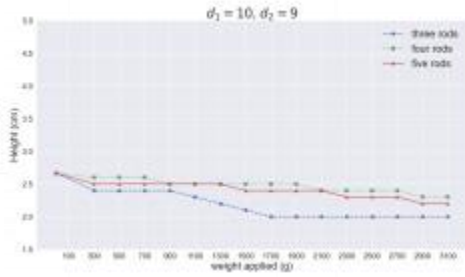
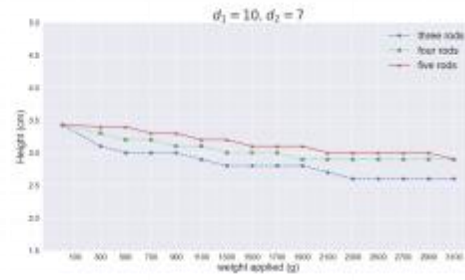
Figure 13. Height Change of Three, Four, and Five Rods Structures under Weight

All the structures can withstand up to 60-100 times of their own weights, see figure 13. The structure drops at a rapid rate with the initial few weights. Then, it reaches a steady state in which the height decreases much slower with very small slope. Due to the limit of the measurement accuracy, the curve exhibits a decreasing behavior in a staircase manner.

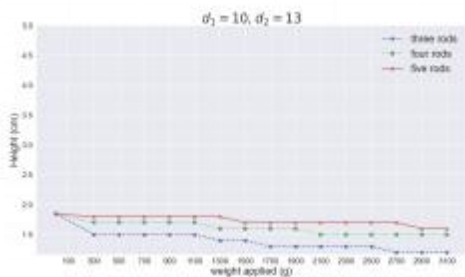
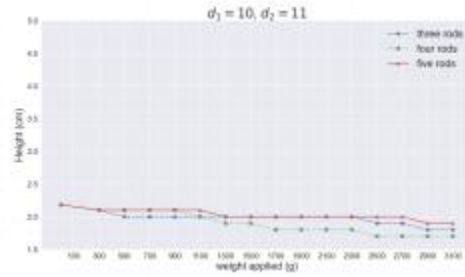
For three rods structures, the curve with $d_2 = 5$ drops so fast initially that it collapses to the curve with $d_2 = 7$. Similarly, the curve with $d_2 = 9$ also collapses to the curve with $d_2 = 11$. This is not the case for four and five rods system, such that there are no crossings between curves and the rank by initial height is same as the rank by final height. Therefore, the four and five rods systems are more stable and rigid than the 3 rod one.



(a) $d_2 = 5$ (b) $d_2 = 7$



(c) $d_2 = 9$ (d) $d_2 = 11$



(e) $d_2 = 13$

Figure 14. Height of Three Dry Rods Structures for Different d_2 Values

In Figure 14, three, four, and five rods structures with the same d_2 are plotted together. Observing figure 14a, the three rods structure with $d_2 = 5$ drops significantly in height, whereas 4 and 5 rods structures nearly retain at the same plateau much higher than 3 rods structures. For bigger values of d_2 , the difference between three, four, and five rods is reduced significantly.

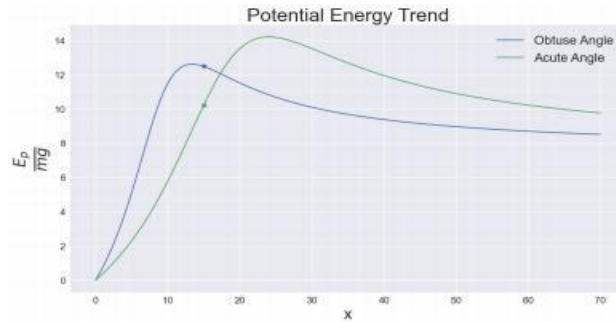
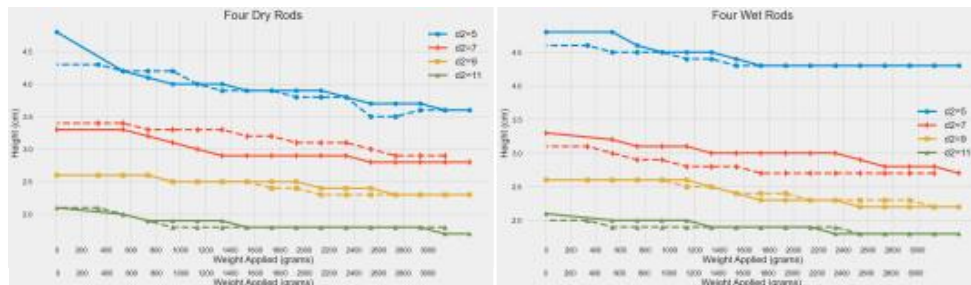


Figure 15. Potential Energy Trend for Acute and Obtuse Angle

One difference between the stability behavior of three and five rods’ structure may be attributed to the potential energy trend. The two neighboring rods of five rods structures form an obtuse angle (figure ??), whereas three rods structures form acute angle (figure ??). The potential energy curves for these two cases are plotted in figure 15 as functions of x (the distance on the lower rod between the contacting point of the rods and the end it touches the ground, see figure 7). A larger x denotes a higher contacting point. Two points are indicated in figure 15 for $x = 15$. The point in case of obtuse angle is on the right side of a peak, showing that it has to go over an energy barrier before sliding down; in the case of acute angle, however, the potential energy is on a steep slope on the left side of a peak, meaning that it is much easier to slide down. Thus, five rods structures are more stable since the barrier of the energy peak prevents it from sliding down.



(a) Three Dry Rods, experiment date August 25th. (b) Three Wet Rods, experiment date August 25th. (c) Four Dry Rods, experiment date August 1st. (d) Four Wet Rods, experiment date August 1st.

Figure 16. Three/Four Dry/Wet Rod under Weight, the Curve with Lighter Color Represent Reformation”

In the height-weight Figure of three rods (Figure 13), multiple metastable states exist. The curve of $d_2 = 5$ jumps to $d_2 = 7$ curve when the first weight is applied. The $d_2 = 9$ curve merges with $d_2 = 11$ under higher weight. We presume that the nest will not be able to retain its original height after removing the weights, so we conducted hysteresis experiment as shown in figure 16. This experiment was performed two months after the first one. The changing weather and environmental conditions may affect the results. This time, we also made comparison experiment between dry and

wet rods. Their friction coefficients and Young's Modulus were measured and listed in table 4.

Table 4. Physical Properties of Dry and wet Rods

	Dry Rods	Wet Rods
Static Friction Coefficient	0.202	0.485
Young's Modulus ($\times 10^9$ Pa)	7.15	5.69

After all fifteen weights are applied, we then remove them one by one to observe the hysteresis loop of the different rod structures. Solid (dotted) curves are the results when applying (removing) weight. In dry rod experiment (figure 16a), the results are mostly similar to figure 13a but different in terms that, this time, the three rod curves for $d_2 = 5, 7, 9$ first merge and then separate afterwards. The four rod curves never intersect. In the wet rod curves for $d_2 = 5, 7$ merge slowly and other curves do not intersect with each other.

Now we look at the hysteresis properties. As we have expected, in figure 16a the curves for $d_2=5, 7$ jump to $d_2=9$ curve, their initial heights are not retained after removing the weights. The wet rod experiment for $d_2=5$ is the same case, see figure 16b.

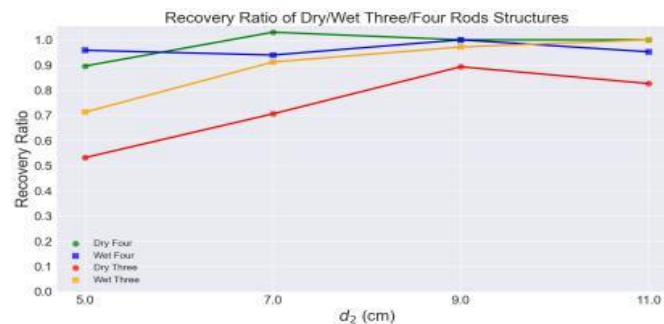


Figure 17. Recovery Ratio of Wet/Dry Three/Four Rods Structures

In Figure 16c, there also exist relatively small hysteresis loops. In some cases, the recovering height might ever be above the original one. Yet, we still regard the structures as an elastic phase approximately. If we define elastic phase as a recovery ratio greater than 90%, then most four rods structures are elastic, whereas the three wet rods structures are elastic when $d_2 \geq 7$, see Figure 17. For the structures not being able to recover to their initial heights, the points that deviate from linearity will be regarded as plastic phase. Thus, applying weight can transfer the structures from plastic phase to elastic phase.

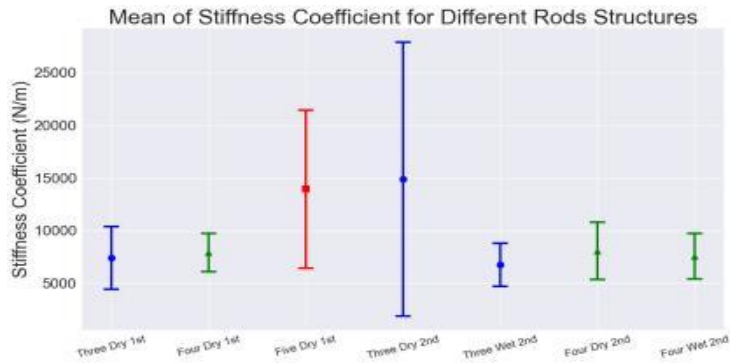


Figure 18. Stiffness Coefficient for Dry/Wet Three/Four Rods

We then define the stiffness coefficient as $k = \frac{\Delta W}{\Delta h}$. The data are obtained by taking the average of the slopes over different d_2 from Figures 13 and 16. Only the linear ranges are used. As shown in figure 18, five rods structures are significantly stiffer than four and three rods structures. The wet structures are less stiff than dry structures because of a lower young's modulus.

3.4 Comparison to Theory

According to theory, applying weight does not change the condition for μ (equation 18) but changed the condition for μ' (equation 31). If friction coefficient with the table cannot support the structure, it will slide down and d_2 will increase.

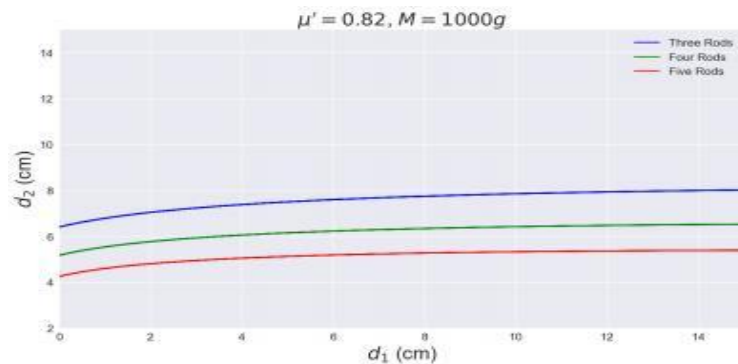


Figure 19. Theoretical Phase Boundary between Stable and Unstable States

Figure 19 is the theoretical phase boundaries between stable and unstable structures for three, four and five rods structures when $\mu' = 0.82$, applied weight $M = 1000g$. The area above each curve is the stable phase and beneath each is the unstable phase. Both the theory (Figure 19) and the experiment (Figure 14) prove five rods structures can remain stable under a lower d_2 . It is not just because of a lower weight per rod, but also because number of rods affect the parameter α (interior angle of a regular polygon), and a bigger α would yield a bigger stability area.

The experiment confirms that the structures will decline rapidly at the beginning and slowly later (Figure 13). Also, the wet rods structures are more stable because of a higher recovery ratio than dry rods (figure 17) and a lower standard deviation of stiffness coefficient (Figure 18) than dry

rods. These two trends can be explained by the condition for minimum μ' which is proportional to factor $\frac{M/n+m/2}{M/n+m}$ (equation 31). The factor ranges from $\frac{1}{2}$ to 1. When M is close to zero, the ratio increases rapidly as M increases, whereas the term would approach 1 as M is sufficiently big. For an insufficient value of μ' , this explains the behavior of the initial rapid decline and later slower decline. In addition, a bigger m (heavier rods) would yield a lower phase boundary, which explains the relatively higher stability of the wet rods.

4. Conclusion

This study discovers a self-supporting bird nest structure constructed by merely packing a few bam-boo rods, with neither container nor fastener. We analyze the stability of the structure under different conditions. For free rods structures (no applied weight or vibration), several conclusions can be derived theoretically. When the coefficient of friction with the ground μ' is sufficient, the stability of the structure can be determined by the condition for μ , which only depends on d_1 and d_2 . A theoretical phase boundary between the stable and unstable states has been obtained at fixed μ with varying d_1 and d_2 . The theoretical phase boundary matched the experiment results well.

We also test the stability of the structure when weights are applied. The threshold μ' underweights would increase by a factor of $\frac{2(M/n+m/2)}{M/n+m}$ in theory. This factor increases quickly at first when applied mass M is small and approaches 1 as M gets bigger. The rods in structures would slide down (height decrease, d_2 increase) to satisfy the condition for μ' . The condition for μ' also included the parameter α , the interior angle of a regular n-gon. A bigger α would yield a smaller threshold μ' , so structures with more rods are more stable. In conclusion, static structures with greater d_2 and a number of rods (five>four>three) are more stable. We also used potential energy analysis to explain the stability of the structures. These theoretical predictions are all verified in the experiment. We also find that wet rod structures are more stable than dry ones. The structures can support up to 100 times of its own weight.

Yet, this study is still an oversimplification compared to bird nests in real life. Unlike the structures in which each rod takes the same weights, rods in real bird nests each have different lengths and diameters. The real nests are not necessarily symmetric. Randomness also exists in the process of bird nest construction. These are points to be investigated in further studies.

References

- Andrea, J. L., & Sidney, R. N. (2010). The Jamming Transition and the Marginally Jammed Solid. *Annual Review of Condensed Matter Physics*, 1(1), 347-369 2010. <https://doi.org/10.1146/annurev-conmatphys-070909-104045>
- Popular Science Matters. (2020). Ice Bomb - Ice Stick Bomb, Challenge Awaits! 2020. Retrieved from <http://www.163.com/dy/article/FL01GAAB05323H3L.html%7D>
- Siobhan, R. (2020). *Why Birds Are the World's Best Engineers*. Retrieved from

- <https://www.nytimes.com/2020/03/17/science/why-birds-are-the-worlds-best-engineers.html%7D>
- Song, L. P., Yu, S., Liu, Y. P., & Li, Z. (2016). Study on Measuring Young's Modulus of Cylindrical Specimens by Bending Method. *Physics Experiment*, 6, 22-26.
- Weiner, N., Bhosale, Y., Gazzola, M., & King, H. (2020). Mechanics of Randomly Packed Filaments—The “Bird Nest” as Meta-Material. *Journal of Applied Physics*, 127, 050902. <https://doi.org/10.1063/1.5132809>
- Yao, X. X., Liu, G. Y., Yang, H. C., Xiao, T., & Zheng, Y. (2024). The motion of a washer on a vertical steel rod. *European Journal of Physics*, 45, 015002. <https://doi.org/10.1088/1361-6404/ad0d89>
- Yashraj, B., Nicholas, W., Butler, A., Seung, H. K., Mattia, G., & Hunter, K. (2022). Micromechanical Origin of Plasticity and Hysteresis in Nestlike Packings. *Physical Review Letters*, 128. <https://doi.org/10.1103/PhysRevLett.128.198003>